*Iron Oxide Nanotubes*

# Single-Crystalline Iron Oxide Nanotubes**

*Chun-Jiang Jia, Ling-Dong Sun,* Zheng-Guang Yan, Li-Ping You, Feng Luo, Xiao-Dong Han, Yu-Cheng Pang, Ze Zhang, and Chun-Hua Yan**

In recent years considerable attention has been focused on one-dimensional nanostructured materials owing to their unique physical properties and potential applications in sensors, magnetics, electric transportation, optics, and even as building blocks for nanoscale devices.[1] In particular, much effort has been devoted to the controllable synthesis of inorganic nanotubes since the discovery of carbon nanotubes in 1991.[2] The synthesis of a number of tubular materials from two-dimensional layered precursors at elevated temperatures, based on a "rolling-up" mechanism, has been reported,[3] such as BN, $V_2O_5$, $WS_2$, and $NiCl_2$. With the development of soft-chemistry synthetic methods, a low-temperature solution approach provides a facile method to produce nanotubes of lamellar compounds,[4] for example InS, Bi, and $Cu(OH)_2$. Nanotubes made from other materials,[5] such as Si, ZnS, $Eu_2O_3$, and GaN, which do not possess 2D layered structures, have also been prepared by employing various templates. However, except for a few examples,[5a,d] the template-assisted method has proved to be unsuitable for the formation of single-crystalline nanotubes. A mild solution strategy has been used[6] to obtain single-crystalline hexagonal prismatic Te nanotubes, but it is difficult to extend this method to the formation of other three-dimensional materials. It is therefore still a challenge to extend the fabrication of single-crystalline tubular nanostructures from lamellar to 3D materials.

Hematite ($\alpha$-$Fe_2O_3$), the most stable iron oxide under ambient conditions, is widely used in catalysts,[7] pigments,[8] sensors,[9] and as the raw material for the synthesis of

[*] C.-J. Jia, Prof. Dr. L.-D. Sun, Z.-G. Yan, F. Luo, Y.-C. Pang, Prof. Dr. C.-H. Yan
State Key Lab of Rare Earth Materials Chemistry and Applications
PKU-HKU Joint Lab in Rare Earth Materials and Bioinorganic Chemistry
Peking University
Beijing 100871 (China)
Fax: (+86) 10-62754179
E-mail: sun@pku.edu.cn
yan@pku.edu.cn

Prof. L.-P. You
Electron Microscopy Laboratory
Peking University
Beijing 100871 (China)

Prof. Dr. X.-D. Han, Prof. Dr. Z. Zhang
Institute of Microstructure & Properties of Advanced Materials
Beijing University of Technology
Beijing 100022 (China)

[**] Grants-in-aid from NSFC (nos. 10374006, 20221101, and 20423005) and MOST of China (no. 2002CB613500) are gratefully acknowledged.

Supporting information for this article is available on the WWW under http://www.angewandte.org or from the author.

  DOI: 10.1002/ange.200463038 

maghemite ($\gamma$-$Fe_2O_3$), which is of great importance as a ferro fluid and in magnetic recording materials. Because of its excellent properties, much attention has been directed to the controlled synthesis of hematite particles. For example, Matijevic and co-workers[10] have prepared monodispersed hematite particles by forced hydrolysis of ferric ions in solution, and Kallay et al.[11] and Sugimoto et al.[12] have synthesized hematite particles with controllable shape and size by a sol–gel method. Recently, much research has been focused on the synthesis of 1D nanostructures, including nanorods,[13] nanowires,[14] nanobelts[15] of hematite, and nanotubes of magnetite,[16] owing to their potential applications in various fields. Herein, we report a rational synthesis of single-crystalline hematite nanotubes by a convenient hydrothermal method, and demonstrate a feasible, large-scale, and controllable synthesis of single-crystalline $Fe_2O_3$ nanostructures. A mechanism for the formation of tubular-structured hematite is proposed in accordance with the morphology investigations carried out by electron microscopy. Different from the mechanism of formation of other inorganic nanotubes reported previously, these hematite nanotubes are formed by a coordination-assisted dissolution process. The presence of phosphate ions is the crucial factor that induces the formation of a tubular structure, which results from the selective adsorption of phosphate ions on the surfaces of hematite particles and their ability to coordinate with ferric ions. Single-crystalline maghemite nanotubes are also obtained by a reduction and re-oxidation process with hematite nanotubes as precursors. This approach not only enriches iron oxide chemistry, but also provides a new strategy to synthesize single-crystalline nanotubes of non-lamellar-structured materials, which could be applicable to the synthesis of other inorganic tubular nanostructures.

The hematite products were synthesized by a solution-phase approach. In a typical experimental procedure, the nanotubes were obtained by the hydrothermal treatment of an $FeCl_3$ solution (0.02 M) in the presence of $NH_4H_2PO_4$ ($7.2 \times 10^{-4}$ M) at 220 °C for 48 h. The morphology of the typical hematite nanotubes obtained was studied by electron microscopy. Figure 1a shows an SEM image of the as-synthesized hematite nanotubes, with a magnified image shown in the inset. The product consists almost entirely of nanotubes with outer diameters of 90–110 nm, inner diameters of 40–80 nm, and lengths of 250–400 nm. Some of the nanotubes have one end open with the other end closed. The phase purity of the products was examined by X-ray diffraction (Figure 1b). All the peaks can be well-indexed to a pure corundum structure (space group $R\bar{3}c$) of hematite (JCPDS: 33-0664).

To provide further insight into the nanostructures of the tubes, analytical TEM investigations were also performed. Figure 2a shows an STEM image of a single hematite tube collected with a high angle annular dark field detector (HAADF) attached to a TEM. The sidewalls of the hematite nanotubes in the STEM images appear brighter as a result of the relatively large number of atoms relative to the other parts of the nanotubes. The compositional line profiles (Figure 2b) probed by energy-dispersive X-ray spectroscopy (EDS) exhibit well-correlated iron and oxygen signals across the tube walls (the arrow in Figure 2a). Figure 2c shows a typical HRTEM image of a single hematite nanotube, and the inset of this figure shows the low-resolution TEM image. The clear lattice image indicates the high crystallinity and single-crystalline nature of the hematite nanotubes. A lattice spacing of 0.460 nm for the (003) planes of the rhombohedral hematite structure along the nanotube can be readily

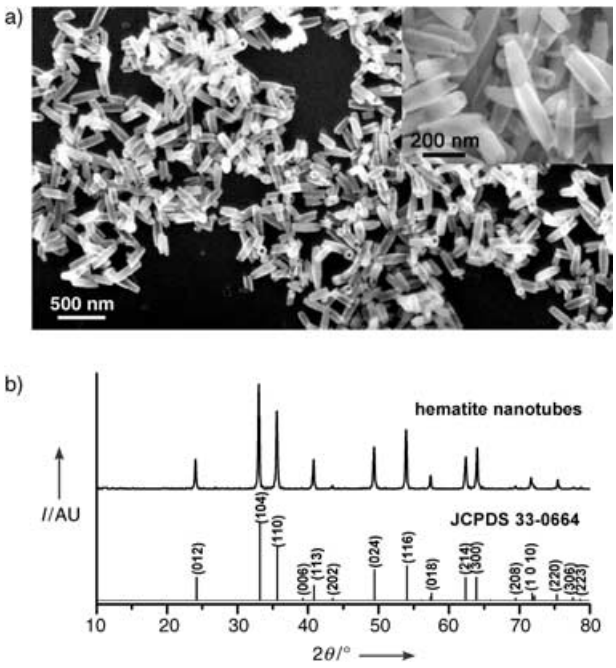


***Figure 1.*** a) Hematite nanotubes imaged with SEM (inset: magnified view) and b) XRD pattern of the hematite nanotubes.

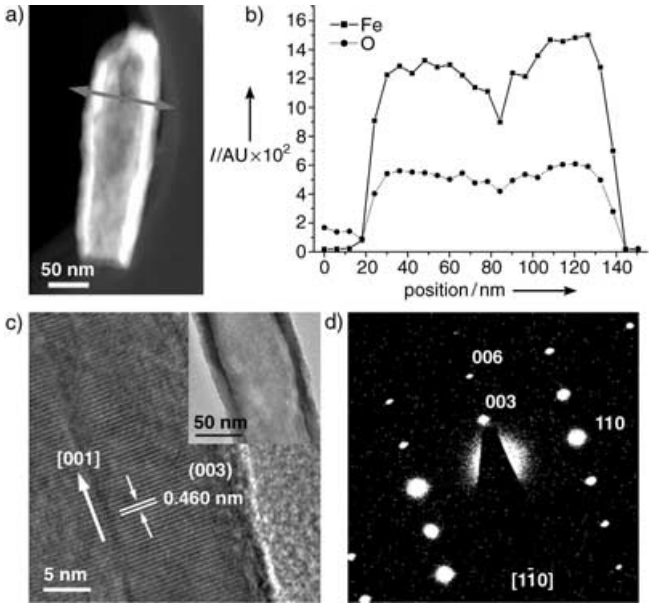


***Figure 2.*** a) STEM image of a single nanotube; b) compositional line profiles across the tube probed by EDS along the line in part a); c) HRTEM image; d) SAED pattern of the single nanotube shown in the inset of part c).

  

resolved. The selective-area electron diffraction (SAED) (Figure 2d) and HRTEM analyses reveal that the nanotubes grow along [001] (*c* axis). The (003) reflection shown in Figure 2d is often forbidden in the corundum structure of hematite, as shown in the XRD patterns (see Figure 1b). We suppose that the observation of the (003) reflection by ED is the result of a double-diffraction effect due to the strong electron scattering.[17]

For a complete view of the formation process of the hematite nanotubes and their growth mechanism, a detailed time-dependent morphology evolution study was conducted at 220 °C (Figure 3a–d). The product obtained after 2 h

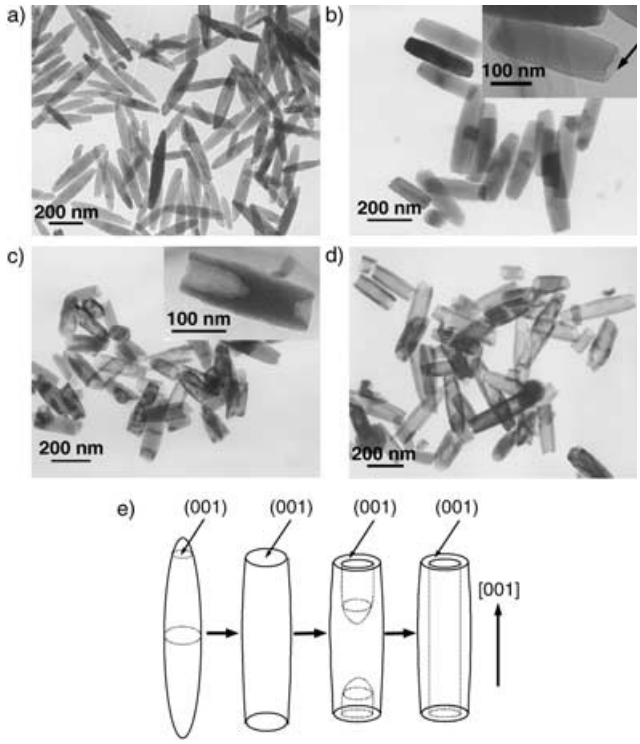


***Figure 3.*** Morphology evolution of the hematite nanotubes with reaction time: TEM images of the products obtained at 220 °C after a) 2 h, b) 8 h, c) 12 h, and d) 48 h; e) schematic illustration of the tube-formation process.

contains spindlelike particles with a diameter of 60–70 nm and a length of 350–450 nm, as has been extensively observed in forced hydrolysis processes.[10,18] Prolonging the reaction time to 8 h gave nanorods with a diameter of about 100 nm and a length of 250–400 nm. The tips of these rods are concave, as can be observed in the inset of Figure 3b. A mixture of rodlike, tubular, and semitubular (inset of Figure 3c) nanostructures was formed after longer reaction times (12 h, Figure 3c). For reaction times of 48 h (Figure 3d), the product consists predominantly of nanotubes that are completely hollow. XRD analysis confirmed the hematite phase of all the above products. HRTEM and SAED analysis of the hematite nanorods and tubes formed at different stages (see Supporting Information) showed that they all grow along the [001] direction, which is consistent with the preferential growth direction of the spindles.

Based on the above time-dependent morphology evolution evidence, the formation process of the nanotubes can be proposed as occurring by "dissolution" of the spindlelike precursors from the tips toward the interior along the long axis, via rodlike nanocrystals and semi-nanotubes, until hollow tubes are formed (Figure 3e). The driving force is the high activity of the sharp spindle tips, which are easily attacked by the protons in acidic solution (pH 1.8). Notably, only part of the interior is dissolved during the formation of hematite nanotubes, and the dissolution is not uniform from spindle to spindle and even for a single spindle (see Figure 3b,c). Furthermore, the diameter of the final nanotubes is larger and the surface is smoother than those of the spindlelike precursors, which indicates that recrystallization on the surface also accompanies the "dissolution" process. This process is similar to that occurring in ZnO, which "etches" from the center of the hexagonal disks to form hexagonal rings.[19]

Although the formation process of the nanotubes has been deduced, the intrinsic cause of the shape transformation from spindle to tube is still unclear. The growth control of hematite nanocrystals by the adsorption of phosphate ions has been extensively studied.[10,18] Our investigations show that phosphate adsorption on the hematite surface takes place, and that these adsorbed phosphate ions cannot be removed by washing (Supporting Information).[20] The adsorption behavior of anions on oxides and hydroxides depends on the surface properties, particularly the surface hydroxy group configuration.[21] The adsorption of phosphate on hematite occurs by reaction with the singly coordinated surface hydroxy groups to form a monodentate or bidentate inner-sphere complex.[22] A hematite crystal has a rhombohedrally centered hexagonal structure of the corundum type with a close-packed lattice in which two thirds of the octahedral sites are occupied by $Fe^{3+}$ ions (see Figure 4a). In a typical crystal unit, each Fe atom is surrounded by six O atoms, whereas each O atom is bound to four Fe atoms. Due to these characteristics of the corundum structure, the surface hydroxy group configuration of the various crystal faces of hematite is quite different.[21] For (001) planes (see Figure 4b), the surface hydroxy functions are all doubly coordinated, whereas for other planes that commonly occur at the surface of natural and artificial hematite crystals, such as the (100), (110), (012), and (104) planes, singly coordinated surface hydroxy groups are present. Therefore, the adsorption capacities and affinities for phosphate to hematite are much lower for the (001) planes than for the others,[22a] and the adsorbed phosphate will protect them from further reaction. Although previous studies[23] have shown that dissolution of hematite does not appear to take place preferentially at specific crystal faces, the selective adsorption of phosphate ions on the crystal planes parallel to the *c* axis other than (001) favors the dissolution along the *c* axis and causes the hematite tube to grow in the [001] direction.

Besides the selective adsorption of phosphate ions at different faces, the coordination effect of phosphate ions with $Fe^{3+}$ ions is another important aspect in the formation of

  

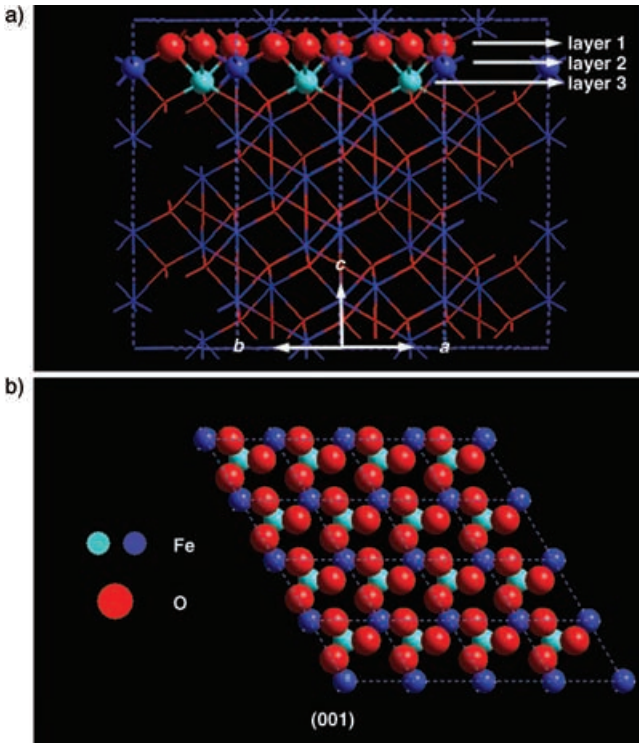


***Figure 4.*** Schematic structures of hematite: a) crystal structure projection on the (110) plane: the repeating elemental sequence is $(O,Fe,Fe)_n$ along the *c* axis; b) crystal structure projection on the O-terminated (001) plane, in which O atoms are all doubly coordinated by Fe atoms. Compared with other planes, the adsorption capacities and affinities for phosphate are much lower for (001) owing to the absence of singly coordinated hydroxy groups.

nanotubes. As for the "dissolution" of the hematite particles, the following reactions take place:

$$Fe_2O_3 + 6\,H^+ \rightarrow 2\,Fe^{3+} + 3\,H_2O \quad (1)$$

$$Fe^{3+} + x\,H_2PO_4^- \rightarrow [Fe(H_2PO_4)_x]^{3-x} \quad (2)$$

The formation of $[Fe(H_2PO_4)_x]^{3-x}$ [Eq. (2)] forces Equation (1) toward the right-hand side and speeds up the dissolution of the hematite particles. Based on the two roles played by phosphate ions during the reaction, we have proposed a coordination-assisted dissolution process for the hematite tube formation during hydrothermal treatment of the spindle precursors in the presence of phosphate ions (see Figure 3e).

Experiments to determine the parameters, other than the reaction time, that are also important for the formation of the nanotubes were carried out. For example, their formation at temperatures lower than 220 °C is not favored as spindle nanocrystals dominate at 180 °C and only a few nanotubes form at 200 °C (Supporting Information). The phosphate ions are essential for the formation of spindlelike hematite, which is the precursor for the formation of the tubular structure. Furthermore, the concentration of phosphate ions should be maintained for the coordination-assisted dissolution process to proceed. If the concentration of phosphate ions is lower than $6.5 \times 10^{-4}$ M, nanorods or only a few nanotubes are obtained instead of large amounts of nanotubes. On the other hand, a relatively large phosphate ion concentration ($> 1.0 \times 10^{-3}$ M) destroys the tubes. Under basic conditions only solid particles are obtained, and the mediation effect of phosphate ions is weak. Moreover, tubular structures are not formed due to the lack of spindle precursors, and the high pH value does not favor the dissolution. Other ions that coordinate to $Fe^{3+}$, like $SO_4^{2-}$, also lead to the "dissolution" of the spindle precursors and formation of the final tubular product. Studies on the formation of other kinds of hematite nanostructures, based on this dissolution process, are still in progress.

Maghemite, and especially its nanostructures,[24] are scientifically interesting and technologically important as a type of magnetic material. We were able to obtain maghemite nanotubes by a reduction and re-oxidation process starting with the hematite nanotubes as precursors. Figure 5a shows an SEM image of the maghemite nanotubes obtained. Compared with the corresponding hematite precursors, the size, tubular structure, and the single-crystal nature are perfectly maintained for maghemite. The XRD patterns of the maghemite nanotubes are shown in Figure 5b; all of them can be well indexed to a pure spinel structure of maghemite

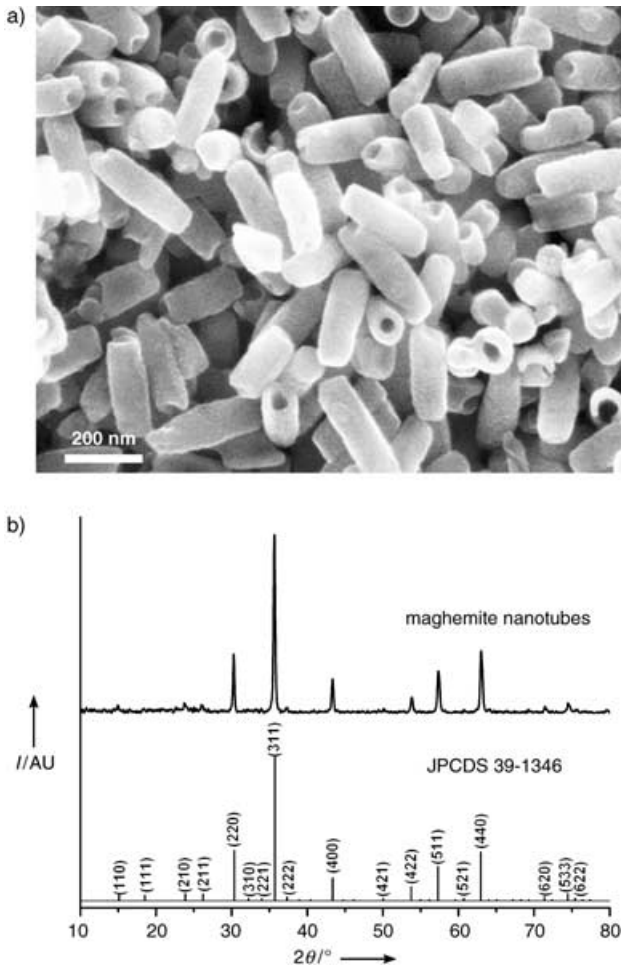


***Figure 5.*** a) SEM image and b) XRD pattern of the maghemite nanotubes.

  

(JCPDS: 39-1346). The sharp peaks confirm the high crystallinity of the products. A study of the magnetic properties of these maghemite nanotubes is still in progress. Both the hematite and maghemite nanotubes provide novel structures for magnetism studies and also have potential applications for the design of novel complex structures[25] and as carriers in biomagnetic sensors, nanomedicine, and catalysis.

In summary, single-crystalline hematite nanotubes have been fabricated by a facile, one-step hydrothermal method. Various experimental conditions, including temperature, additives, pH value, and reaction time for the growth of hematite nanocrystals were investigated. Based on the evidence of electron microscope images, the formation mechanism of tubular-structured hematite has been proposed as a coordination-assisted dissolution process. The presence of phosphate ions in this process is crucial because of their different adsorption ability on the different crystal planes of hematite and a coordination effect with $Fe^{3+}$, which induces the preferential dissolution of the hematite spindle precursors along the long axis from the tips down to the interior. Maghemite nanotubes have also been obtained in a reduction and re-oxidation processes of these hematite precursors. These results not only enrich the tubular nanostructures of inorganic compounds, but also provide a new strategy to synthesize single-crystalline nanotubes of nonlamellar-structured materials, which could be applicable to the synthesis of other inorganic tubular nanostructures.

## Experimental Section

The hematite nanotubes were fabricated by hydrothermal treatment of a mixture of $FeCl_3$ and $NH_4H_2PO_4$ solutions. In a typical experimental procedure, 3.20 mL of aqueous $FeCl_3$ solution (0.5 M) and 2.88 mL of aqueous $NH_4H_2PO_4$ solution (0.02 M) were mixed with vigorous stirring. Distilled water was then added to a final volume of 80 mL. After stirring for ten minutes, the mixture was transferred into a Teflon-lined stainless-steel autoclave with a capacity of 100 mL for hydrothermal treatment at 220 °C for 48 h. After the autoclave had cooled down to room temperature naturally, the precipitate was separated by centrifugation, washed with distilled water and absolute ethanol, and dried under vacuum at 80 °C. The parameters that are essential for the tube formation were studied by varying temperature, concentration of $NH_4H_2PO_4$, pH value, and the reaction time.

Maghemite nanotubes were obtained by a reduction and re-oxidation of the hematite nanotube precursors. The dried hematite powders were annealed in a furnace at 360 °C under a continuous hydrogen gas flow for 5 h. Then, the gas flow was stopped, the powder exposed to air, and the furnace temperature decreased to 240 °C over 2 h.

The powder XRD patterns were recorded with a Rigaku D/MAX-2000 diffractometer using Cu $K_\alpha$ radiation ($\lambda = 1.5418$ Å). SEM images were obtained with a DB-235 focused ion beam (FIB) system. TEM images were recorded with a JEOL 200CX transmission electron microscope at a working voltage of 160 kV. HRTEM, EDS, and STEM were performed with a Philips Tecnai F30 FEG-TEM operating at 300 kV. IR spectra were obtained with a Nicolet Magna 750 FTIR spectrometer at a resolution of 4 $cm^{-1}$ with a Nic-Plan IR microscope.

Received: December 22, 2004
Published online: June 15, 2005

**Keywords:** hematite · hydrothermal synthesis · iron · materials science · nanotubes

[1] a) J. T. Hu, T. W. Odom, C. M. Lieber, *Acc. Chem. Res.* **1999**, *32*, 435; b) G. R. Patzke, F. Krumeich, R. Nesper, *Angew. Chem.* **2002**, *114*, 2554; *Angew. Chem. Int. Ed.* **2002**, *41*, 2446; c) F. Favier, E. C. Walter, M. P. Zach, T. Benter, R. M. Penner, *Science* **2001**, *293*, 2227; d) Y. N. Xia, P. D. Yang, Y. G. Sun, Y. Y. Wu, B. Mayers, B. Gates, Y. D. Yin, F. Kim, Y. Q. Yan, *Adv. Mater.* **2003**, *15*, 353; e) Y. C. Sui, R. Skomski, K. D. Sorge, D. J. Sellmyer, *Appl. Phys. Lett.* **2004**, *84*, 1525.
[2] S. Iijima, *Nature* **1991**, *354*, 56.
[3] a) N. G. Chopra, R. J. Luyken, K. Cherrey, V. H. Crespi, M. L. Cohen, S. G. Louie, A. Zettl, *Science* **1995**, *269*, 966; b) P. M. Ajayan, O. Stephan, P. Redlich, C. Colliex, *Nature* **1995**, *375*, 564; c) R. Tenne, L. Margulis, M. Genut, G. Hodes, *Nature* **1992**, *360*, 444; d) Y. R. Hacohen, E. Grunbaum, R. Tenne, J. Sloan, J. L. Hutchison, *Nature* **1998**, *395*, 336.
[4] a) J. A. Hollingsworth, D. M. Poojary, A. Clearfield, W. E. Buhro, *J. Am. Chem. Soc.* **2000**, *122*, 3562; b) Y. D. Li, J. W. Wang, Z. X. Deng, Y. Y. Wu, X. M. Sun, D. P. Yu, P. D. Yang, *J. Am. Chem. Soc.* **2001**, *123*, 9904; c) W. X. Zhang, X. G. Wen, S. H. Yang, Y. Berta, Z. L. Wang, *Adv. Mater.* **2003**, *15*, 822.
[5] a) J. Q. Hu, Y. Bando, Z. W. Liu, J. H. Zhan, D. Golberg, T. Sekiguchi, *Angew. Chem.* **2004**, *116*, 65; *Angew. Chem. Int. Ed.* **2004**, *43*, 63; b) X. D. Wang, P. X. Gao, J. Li, C. J. Summers, Z. L. Wang, *Adv. Mater.* **2002**, *14*, 1732; c) G. S. Wu, L. D. Zhang, B. C. Cheng, T. Xie, X. Y. Yuan, *J. Am. Chem. Soc.* **2004**, *126*, 5976; d) J. Goldberger, R. R. He, Y. F. Zhang, S. W. Lee, H. Q. Yan, H. J. Choi, P. D. Yang, *Nature* **2003**, *424*, 599.
[6] B. Mayers, Y. N. Xia, *Adv. Mater.* **2002**, *14*, 279.
[7] A. S. S. Brown, J. S. J. Hargreaves, B. Rijniersce, *Catal. Lett.* **1998**, *53*, 7.
[8] R. M. Cornell, U. Schwertmann, *The Iron Oxides. Structure, Properties, Reactions, Occurrence and Uses*, VCH, Weinheim, **1996**, p. 464.
[9] H. T. Sun, C. Cantalini, M. Faccio, M. Pelino, M. Catalano, L. Tapfer, *J. Am. Ceram. Soc.* **1996**, *79*, 927.
[10] M. Ozaki, S. Kratohvil, E. Matijevic, *J. Colloid Interface Sci.* **1984**, *102*, 146.
[11] N. Kallay, I. Fischer, E. Matijevic, *Colloids Surf.* **1985**, *13*, 145.
[12] T. Sugimoto, K. Sakata, *J. Colloid Interface Sci.* **1992**, *152*, 587.
[13] L. Vayssieres, N. Beermann, S.-E. Lindquist, A. Hagfeldt, *Chem. Mater.* **2001**, *13*, 233.
[14] a) Y. Y. Fu, J. Chen, H. Zhang, *Chem. Phys. Lett.* **2001**, *350*, 491; b) Y. J. Xiong, Z. Q. Li, X. X. Li, B. Hu, Y. Xie, *Inorg. Chem.* **2004**, *43*, 6540.
[15] X. G. Wen, S. H. Wang, Y. Ding, Z. L. Wang, S. H. Yang, *J. Phys. Chem. B* **2005**, *109*, 215.
[16] Z. Q. Liu, D. H. Zhang, S. Han, C. Li, B. Lei, W. G. Lu, J. Y. Fang, C. W. Zhou, *J. Am. Chem. Soc.* **2005**, *127*, 6.
[17] P. Hirsch, A. Howie, R. B. Nicholson, D. W. Pashley, M. J. Whelan, *Electron Microscopy of Thin Crystals*, Robert E. Krieger, Huntington, New York, **1977**, p. 117.
[18] a) T. Sugimoto, A. Muramatsu, K. Sakata, D. J. Shindo, *J. Colloid Interface Sci.* **1993**, *158*, 420; b) M. Ocaña, M. P. Morales, C. J. Serna, *J. Colloid Interface Sci.* **1995**, *171*, 85.
[19] F. Li, Y. Ding, P. X. Gao, X. Q. Xin, Z. L. Wang, *Angew. Chem.* **2004**, *116*, 5350; *Angew. Chem. Int. Ed.* **2004**, *43*, 5238.
[20] N. J. Reeves, S. Mann, *J. Chem. Soc. Faraday Trans.* **1991**, *87*, 3875.
[21] V. Barrón, J. Torrent, *J. Colloid Interface Sci.* **1996**, *177*, 407.
[22] a) X. Huang, *J. Colloid Interface Sci.* **2004**, *271*, 296; b) M. I. Tejedor-Tejedor, M. A. Anderson, *Langmuir* **1990**, *6*, 602; c) J. D. Russell, R. L. Parfitt, A. R. Fraser, V. C. Farmer, *Nature* **1974**, *248*, 220.

  

[23] R. M. Cornell, R. Giovanoli, *Clay Miner.* **1993**, *28*, 223.
[24] a) S. J. Park, S. Kim, S. Lee, Z. G. Khim, K. Char, T. Hyeon, *J. Am. Chem. Soc.* **2000**, *122*, 8581; b) K. Woo, H. J. Lee, J. P. Ahn, Y. S. Park, *Adv. Mater.* **2003**, *15*, 1761; c) P. Tartaj, T. Gonzalez-Carreno, C. J. Serna, *Adv. Mater.* **2004**, *16*, 529.
[25] a) Y. Kusano, M. Fukuhara, T. Fujii, J. Takada, R. Murakami, A. Doi, L. Anthony, Y. Ikeda, M. Takano, *Chem. Mater.* **2004**, *16*, 3641; b) P. Ball, *Nature* **2004**, *431*, 524.

  